FlatChem 36 (2022) 100447

Contents lists available at ScienceDirect

FlatChem

journal homepage: www.sciencedirect.com/journal/flatchem

Nano-LED driven phase change evolution of layered chalcogenides for Raman spectroscopy investigations

Martin Mikulics [a,b,*], Roman Adam [c], Roman Sobolewski [d,e], Sarah Heidtfeld [c,f], Derang Cao [g], Daniel E. Bürgler [c], Claus M. Schneider [c,f,h], Joachim Mayer [a,b], Hilde Helen Hardtdegen [a,b,*]

[a] Ernst Ruska-Centre for Microscopy and Spectroscopy with Electrons (ER-C-2), Forschungszentrum Jülich GmbH, D-52425 Jülich, Germany
[b] Jülich-Aachen Research Alliance, JARA, Fundamentals of Future Information Technology (JARA-FIT), Jülich, Germany
[c] Peter Grünberg Institute (PGI-6), Forschungszentrum Jülich, 52425 Jülich, Germany
[d] Department of Electrical and Computer Engineering and Department of Physics and Astronomy, University of Rochester, Rochester, NY 14627-0231, USA
[e] Laboratory for Laser Energetics, University of Rochester, Rochester, NY 14623, USA
[f] Faculty of Physics, University of Duisburg-Essen, Duisburg 47048, Germany
[g] College of Physics, National Demonstration Center for Experimental Applied Physics Education, Qingdao University, 266071 Qingdao, China
[h] Department of Physics and Department of Electrical Engineering, University of Southern California, Los Angeles, CA, USA

ARTICLE INFO

Keywords:
Layered chalcogenides
Crystalline trigonal $Ge_1Sb_2Te_4$
Phase-change evolution
Nano-LEDs
Raman spectroscopy

ABSTRACT

We present a device driving testing platform based on vertically integrated nano light emitting diodes (nano-LEDs). The nano-LEDs with a peak wavelength emission centered at ~ 445 nm were arranged in arrays and conditioned using a laser-micro-annealing process to individually tune their intensity. They were coupled with freestanding monocrystalline $Ge_1Sb_2Te_4$ nano-membranes with three different thicknesses (~40, ~ 60 and ~ 90 nm) with the aim of initializing ultrafast switching processes and of observing phase changed states simultaneously by Raman spectroscopy. Raman spectroscopy studies reveal that the optical pulses emitted from the nano-LEDs induce substantial, local changes in the nano-membranes' states of the $Ge_1Sb_2Te_4$ layered material. Beside the crystalline state in non-exposed areas (as-grown material), amorphous and different intermediate states were identified in exposed areas as island-like structures with diameters ranging from ~ 300 nm up to ~ 1.5 μm. The latter confirms the nano-LEDs' emission role in both near- and far-field regimes, depending on the distance between nano-LED and nano-membrane, for driving i.e. inducing the phase change process. The results presented demonstrate the suitability and potential of the vertically integrated nano-LEDs as the key components for a testing platform/for electro-optical convertors driving phase change processes in optically active media. They could also play an important role in the development of future, e.g., non-volatile data storage as well as in optical and neuromorphic computing architectures based on transmistor devices.

Introduction

Chalcogenide phase change materials (PCMs) – for example GeTe and GeSbTe alloys - play an important role in a plethora of applications such as in resistive random access memories (ReRAM) [1–3], optical data disc technology [4], and further alternative application examples [5–17]. Furthermore, it was already proposed that such chalcogenide materials could play an essential role also in future neuromorphic computing developments [18] as well as in novel optical computing architectures based on transmistor devices presented in our previous work [19–21]. These applications utilize the unique properties of this class of materials, that a change in their structural properties, i.e. a change of phase [22], leads to a large change in resistivity [23] and in optical characteristics such as refractive index [24] and absorption coefficient. In the thermodynamically stable form [25] the above mentioned alloys crystallize in a layered trigonal structure. The monocrystallinity of such layered alloys renders them important for further applications such as in energy storage and conversion [26–29], spintronic emitters [30,31], as well as active medium in all-optical switches implemented in transmistor devices [19,20]. The preparation of monocrystalline films of one of the GeSbTe alloys on Si substrates - $Ge_1Sb_2Te_4$ [32,33] – by epitaxy enables the determination of further

* Corresponding authors at: Ernst Ruska-Centre for Microscopy and Spectroscopy with Electrons (ER-C-2), Forschungszentrum Jülich GmbH, D-52425 Jülich, Germany.
E-mail addresses: m.mikulics@fz-juelich.de (M. Mikulics), h.hardtdegen@fz-juelich.de (H.H. Hardtdegen).

https://doi.org/10.1016/j.flatc.2022.100447
Received 2 September 2022; Received in revised form 2 November 2022; Accepted 8 November 2022
Available online 12 November 2022

characteristics of $Ge_1Sb_2Te_4$ [20]. Additionally, it allows the preparation of free-standing membranes and their integration into coplanar strip lines. Thus, a better understanding of charge transport related phenomena and the optical and electrical characterization of their intrinsic nanostructure attributes becomes possible [34].

The determination of the critical heat for such layered chalcogenides on the one hand (i.e. the heat above which degradation of the material sets in) and the knowledge on how to prevent thermal damage on the other hand will play an essential role in the reliability and long-term operation of devices for many applications. Furthermore, it is important to know, when a structural change of the material sets in at the earliest stage (which we call the minimal initialization heat) and when the amorphous phase is reached (i.e. the minimum heat level for phase change). These characteristics are important in especially layered chalcogenide materials which can easily deteriorate and/or are prone to phase changes. Therefore, compact and non-invasive optical characterization methods are mandatory.

Light emitting diodes with lateral dimensions in the nanometer range (nano-LEDs) represent a core component for the next generation of on chip optical communication, integrated photonics quantum technologies, highly resolved illumination microscopy and advanced near-field lithographical techniques [35,36]. Previously, we have demonstrated that GaN based nano-LEDs are promising multi-functional light emitting devices, which can be used for hybrid single photon sources as well as light detectors, and energy-saving devices [37–40]. The monolithic integration of GaN-based devices such as HEMT-LEDs [41,42] provide the multi-functionality for achieving simpler and efficient micro-LED display designs as well as other opto-electronic applications. Nevertheless, there still is a lack of attention to device architectures suitable for reliable and long-term operated nano-LED driving layouts. Recent developments in III-nitride technologies [36,43–62] are significant also for the development of suitable optical device architectures - especially for driving nano-LED structures. Therefore, unconventional device concepts based on current group III-nitride device technologies represent one possible route towards low energy consuming and efficient nano-LED integrated electro-optical convertors.

Here, we report on an alternative application for III-nitride based nano-LEDs in arrays: the provision of a testing platform. It consists of individually conditioned nano-LED optical sources [63] integrated into a vertical device testing layout enabling the local induction of structural phase changes and the simultaneous study of their evolution by Raman spectroscopy. In this work we employed the testing platform to drive and investigate the phase change evolution in layered chalcogenide $Ge_1Sb_2Te_4$ nano-membranes. The nano-LEDs were conditioned after their fabrication by the lately described laser-micro-annealing process for III-nitride based LEDs [63] (also employed for other 2D and layered material structures [64,65]) allowing an individual tunability of their characteristics. The testing platform is presented schematically in Fig. 1. $Ge_1Sb_2Te_4$ nano-membranes with three different thicknesses were transferred directly after growth from their parent substrate to the testing nano-LED platform with the help of transfer techniques described and developed by our group earlier [34,66–68]. This testing approach can be implemented to correlatively characterize complex problems related to reliability and long-term operation of devices brought up, for example, by layered chalcogenide materials.

Experimental

Material synthesis of layered trigonal $Ge_1Sb_2Te_4$

Thin epitaxial and monocrystalline $Ge_1Sb_2Te_4$ films of ~ 40 nm, ~ 60 nm and ~ 90 nm thickness were deposited by metalorganic vapor phase epitaxy (MOVPE) in a home built reactor [20]. The carrier gas nitrogen, which also served as the reaction ambient, was used to transport the precursor compounds digermane (10 % in H_2), triethylantimony and diethyltellurium to the reactor. The carrier gas bubbles

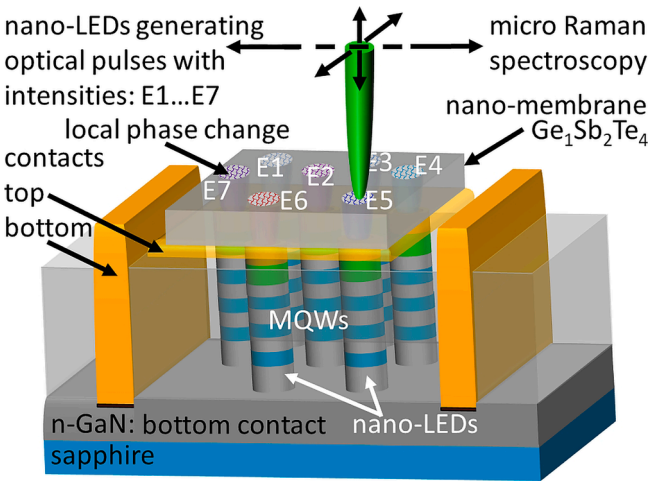

Fig. 1. Principal schematics of the nano-LED structures integrated into the vertical device layout for DC and HF characterization. The nano-LEDs form an array with seven different annealing conditions: annealed locally from E1 to E7 (with increasing laser annealing time). The LEDs' electroluminescence (EL) intensity becomes higher according to the laser-micro-annealing (LMA) process carried out [63]. For the sake of material testing by micro-Raman spectroscopy, the $Ge_1Sb_2Te_4$ nano-membrane was transferred and positioned on top of the nano-LED array. The platform enables the simultaneous local induction of structural phase changes and the study of the evolution by Raman spectroscopy.

through the liquid metalorganic precursors and saturates with their respective vapor pressures. Growth was carried out at 450 °C, 50 hPa reactor pressure and at growth rate of ~ 100 nm/h on silicon (1 1 1) substrates after having removed their native oxide with a dip in 1 % HF and a subsequent annealing procedure. Further details can be found in [32]. These thin films formed the basis for the nano-membranes, which were detachable from the substrate due to the film's layered nature. The obtained epitaxial $Ge_1Sb_2Te_4$ crystallizes in the thermodynamically stable trigonal phase in the space group R $\bar{3}$m. It is characterized by seven alternating anion and cation layer blocks separated by (van der Waals) gaps. The Ge and Sb atoms are statistically distributed on the cation layer site [25] and are coordinated by Te in defective octahedra. These layer blocks are oriented parallel to the Si growth template surface [33]. Fig. 2 depicts the high-angle annular dark-field scanning transmission electron microscopy image (HAADF-STEM) of the layered chalcogenide. The cation, anion and van der Waals gap positions are indicated. For this chalcogenide, our testing platform with nano-LEDs was used.

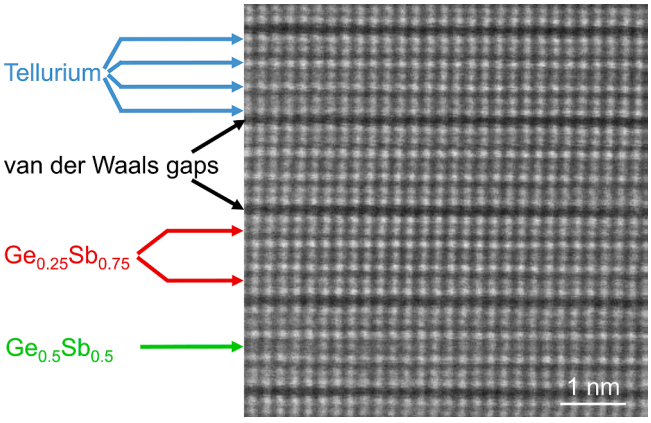

Fig. 2. High-angle annular dark-field scanning transmission electron microscopy image (HAADF-STEM) of the studied layered chalcogenide $Ge_1Sb_2Te_4$ reported previously by Hardtdegen et al. [33] indicating the cation, anion and van der Waals gap positions.

Driving and testing platform based on vertically integrated nano-LEDs

In the following, SEM images (Fig. 3) of our nano-LED testing platform / the electro-optical convertors are presented. The nano-LEDs are functionally arranged and integrated in a vertical device layout suitable for HF operation. This device concept allows for a very flexible integration process with conventionally used optoelectronic devices and circuits as well as optical interconnects serving as an "interface" for data transfer and communication systems. Our concept is not limited to layered chalcogenide materials. It could also be implemented and integrated with a large range of other optically active materials. After the fabrication of the nano-LEDs in arrays [38], they were individually conditioned using the 325 nm line of a continuous wave (cw) HeCd laser: a constant laser power (~ 0.8 kW/cm^2) was employed, with which a successful local annealing had been demonstrated and the annealing time was varied between 2 s and 15 s [63]. By doing so, an array of nano-LEDs intentionally emitting with different emission intensities is achieved, i.e. the electroluminescence of the III-nitride nano-LEDs can be tuned. Since we know, how and where the individual nano-LEDs were conditioned, we were able to directly relate the respective nano-LED position to the site where the material is tested. The testing platform is then ready for material characterization.

The nanostructures – in this case a $Ge_1Sb_2Te_4$ nano-membrane - can be transferred to the testing platform and positioned with the help of a quartz-glass micro-pipette connected to a 3D micromanipulator system. Details to this enhanced transfer technique were presented earlier [66–70]. They were already used for the fabrication of ultrafast femto- and picosecond photoswitches, photodetectors and THz sources [66,71]. The procedure is suitable for separating thin semiconductor films for switches, mesostructures [67], nano-membranes [34] and related nano- / micro-meter sized objects from their native substrates, defining the structure and transferring the nanostructure from the native substrate to a host substrate.

The positioning procedure for the nano-membranes was extensively optimized to ensure that the intrinsic material-structure properties were not unintentionally altered. Fig. 4 presents a detail of nano-membrane structures defined lithographically and after the Ar ion beam etching (IBE) process. Special attention has to be paid to the mechanical stability of such optically active nano-membrane structures. As it can be seen from Fig. 4, the transfer of the single nano-membranes could lead to mechanical damage. Fig. 5 presents exemplary images of the $Ge_1Sb_2Te_4$ nano-membrane transferred to the nano-LED testing platform.

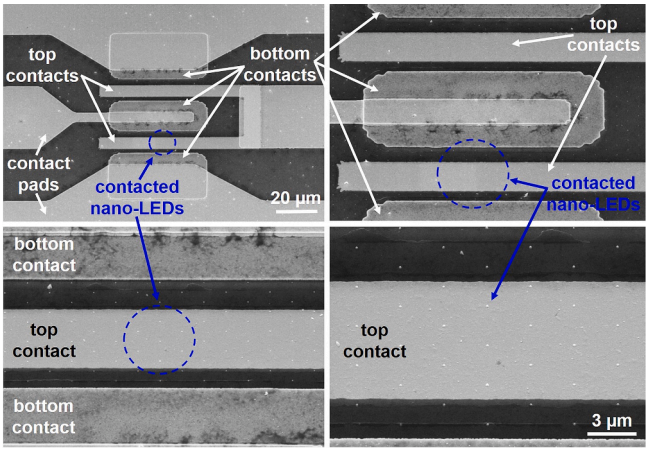

Fig. 3. Exemplary SEM images of fully integrated nano-LED structures in a device layout suitable for DC and HF characterization and details with different magnifications exhibiting the array of nano-LEDs with a transparent Ni/Au (5/5 nm) top contact and annealed Ti/Al/Ni/Au bottom contacts.

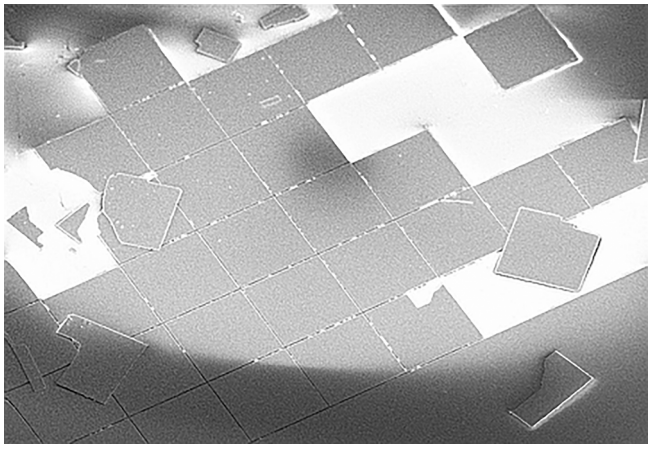

Fig. 4. Example of the nano-membrane structures after the structuring process and subsequent transfer to the insulating sapphire (interim storage) substrate. The structures were covered with photoresist to ensure primary protection during the etching process. The applied protective photoresist layer serves additionally to improve the nano-membrane structural integrity and will be removed after positioning at the testing platform (presented in the following Fig. 5).

Optical characterization

A homemade signal generator was used for the generation of 20 ns electrical pulses driving the nano-LED structures integrated in the testing platform / the electro-optical convertors. As a result, the generated nano-LEDs' optical pulses induced the phase change evolution in the chalcogenide nano-membranes, which was simultaneously detected by micro-Raman spectroscopy. The ~ 20 ns optical pulses with energies in the range between ~ 0.1 pJ and ~ 30 pJ enabled the phase change evolution also up to the undercooled amorphous liquid phase and beyond. These values for optical switching are sufficient, depending on the spot size i.e. illuminated area, and comparable to energy densities necessary for the phase change initialization previously reported in [11,14,73]. Micro-electroluminescence (EL) studies on the conditioned nano-LED structures with a diameter of ~ 100 nm were performed in the 5 V bias voltage DC regime. The recorded EL spectra are presented in Fig. 6.

The nano-membranes were characterized by micro-Raman spectroscopy to confirm structural (phase) changes in the nano-membrane. To this end, an InVia FSM-REFLEX confocal Raman microscope (Renishaw) in backscattering geometry was used, which was equipped with a frequency-doubled Nd:YAG laser (532 nm, 50 mW) and a CCD detector. The power applied and magnification of the employed objective were 0.5 mW and 100X, respectively. Spectra were recorded in the range between ~ 80 cm^{-1} and ~ 200 cm^{-1}. Prior to the studies, the spectra were referenced according to the laser peak position at 0 cm^{-1}, the spectrometer was referenced by acquiring a spectrum of Si, which was referenced to the transverse optical phonon at 521 cm^{-1}.

Results and discussion

The EL of the nano-LEDs in the arrays was characterized at room temperature for several different LMA times. Representative spectra are presented in Fig. 6(a). The nano-LEDs' peak emission is centered at ~ 445 nm. Following the applied conditioning process i.e. the annealing time, the intensity of the nano-LEDs' EL becomes higher [63]. A representative mapping of the electroluminescence intensity (performed at 445 nm) is presented in Fig. 6(b) showing, that the tuning of the LED intensity is successful.

Subsequently, $Ge_1Sb_2Te_4$ nano-membranes with three different thicknesses were placed on the nano-LED array platform, the nano-LEDs

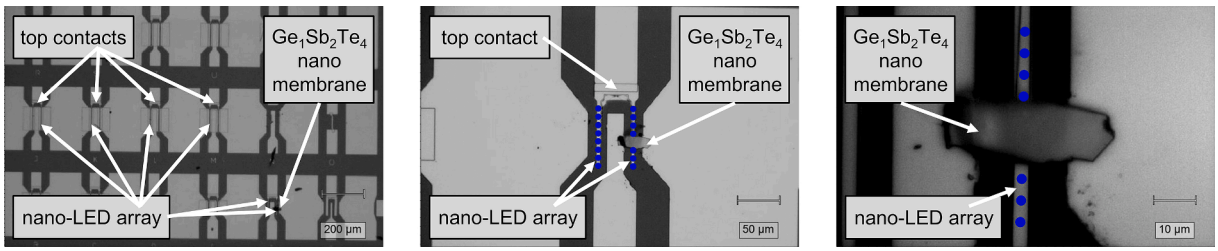

Fig. 5. Exemplary optical microscope images of a $Ge_1Sb_2Te_4$ nano-membrane transferred to one of the nano-LED testing platforms i.e. to the electro-optical (EO) convertors in three different magnifications. Blue optical pulses are only an artistic illustration and a guide to the eye. The device layout (contact pads) of the presented testing units is suitable for operation up to ~ 100 GHz and is based on already developed HEMT technology previously reported [72].

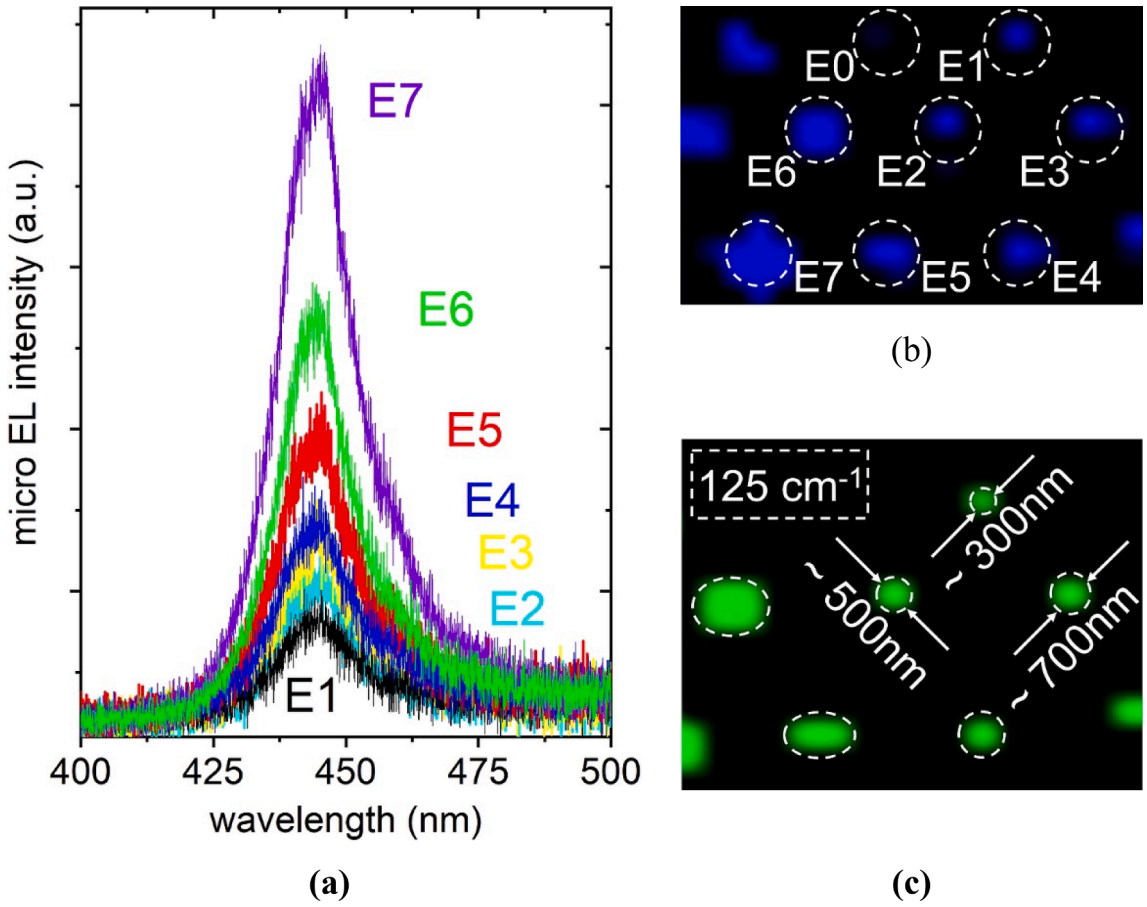

Fig. 6. (a) Representative micro-EL spectra of single nano-LED structures in an array with seven exemplary different intensities E1… E7 (b) respective micro-EL mapping at the central emitted wavelength of 445 nm performed on the conditioned (locally annealed) nano-LEDs arranged hexagonally in an array and compared with their non-locally annealed nano-LED counterpart (E0); the nano-LEDs' EL intensity becomes higher according to the LMA conditioning process time used [63]. (c) Example of a micro-Raman mapping of a ~ 90 nm thick $Ge_1Sb_2Te_4$ nano-membrane demonstrating the effect of different nano-LED conditioning / intensities on the Raman spectra recorded from the $Ge_1Sb_2Te_4$ nano-membrane placed on the testing platform i.e. above the nano-LEDs. The black area relates to crystalline non-phase changed material (~125 cm^{-1}).

of which were conditioned as presented in Fig. 6. The nano-LEDs can induce structural phase changes (in a bottom-up geometry), whilst the changes are simultaneously observed by Raman spectroscopy. Fig. 6(c) depicts an example of a micro-Raman mapping of the $Ge_1Sb_2Te_4$ nano-membrane demonstrating the effect of different nano-LED intensities on the $Ge_1Sb_2Te_4$ nano-membrane placed on the testing platform i.e. above the nano-LEDs. The black area relates to crystalline non phase changed material. The purpose of the Raman study is to determine the minimal initialization heat for first structural changes, the minimal heat level at which the amorphous phase is reached (i.e. still reversible structural changes) and the critical heat above which the material degrades (irreversibly) for such layered chalcogenides. Representative Raman spectra for a 90 nm thick $Ge_1Sb_2Te_4$ nano-membrane are shown in Fig. 7. Spectra were recorded before excitation (below E0), then for several different consecutively increasing emission intensities applied to the nano-membrane. The signature of the crystalline phase (E0,E1) is characterized by a broad band of vibrational modes [74] starting at ~ 100 cm^{-1} and ending around 175 cm^{-1} [20]. A local maximum in the broad band is found at ~ 125 cm^{-1}. This observation of the broad band is most probably related to the structure of the crystalline trigonal $Ge_1Sb_2Te_4$ in which Ge and Sb statistically occupy the octahedral sites, leading to distortions of the octahedra [33] and therefore differences in bond lengths [24,75] within the (Ge,Sb)Te_6 octahedra. Furthermore, the relatively low Raman intensity may be related to the quasi-metallic

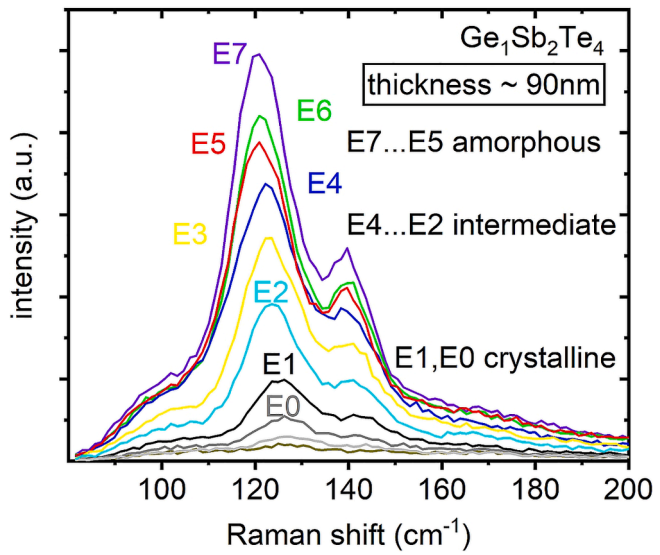

Fig. 7. Representative Raman spectra collected at different positions locally on the $Ge_1Sb_2Te_4$ nano-membrane. Different intensities from the nano-LED structures induce different degrees in the evolution of phase change: an increasing distinction of the bands is observed and a main band evolving from ~ 125 cm^{-1} forms from crystalline (E0,E1) through intermediate states (E2-E4) to amorphous states at ~ 120 cm^{-1} (E5-E7).

appearance of the membranes partially reflecting the nano-LED radiation. As the emission energy increases, distinct modes evolve from the broad band and an additional band appears at ~ 139 cm^{-1}. Different polymorphs can develop [7,76] and intermediate states [16] may evolve (E2–E4). In the amorphous phase (E5-E7), a homogenization of bond lengths occurs, which is then the reason for the observation of the distinct respective bands.

A decrease of the Raman shift of the most intense Raman mode is observed from the crystalline phase (~ 125 cm^{-1}) to the amorphous phase (~ 120 cm^{-1}). This decrease can be used to determine the minimal heat level at which the amorphous phase is reached (i.e. reversible structural changes are induced) for trigonal epitaxial $Ge_1Sb_2Te_4$.

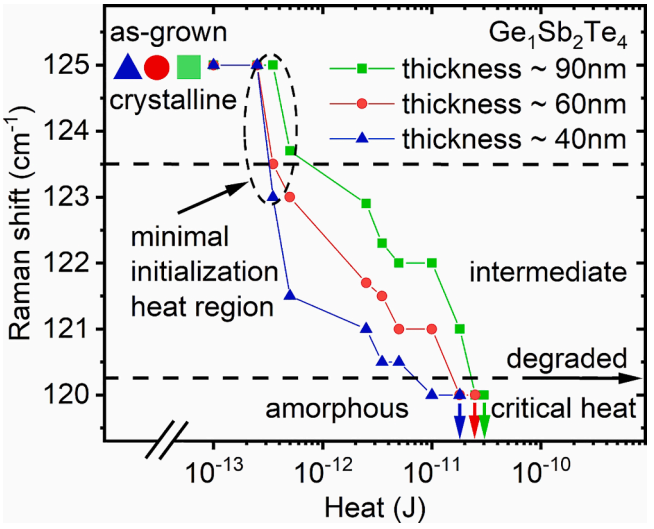

Fig. 8. Raman shift versus heat. The starting point of the phase change and the end point is characterized by the Raman shift ~ 125 cm^{-1} and ~ 120 cm^{-1}, respectively which is independent on the thickness of the membrane. The evolution of phase change is characterized by intermediate states i.e. intermediate Raman shifts. The heat at which structural changes are induced, in contrast, depends on the thickness of the membrane.

The Raman shift versus heat (generated by the nano-LED optical pulses) dependence is presented in Fig. 8 for three different nano-membrane thicknesses. The respective Raman shift remains constant for a specific phase i.e. the crystalline or the amorphous. The onset of phase change is, in contrast, dependent on the thickness of the membrane. Hence, the heat necessary to attain the amorphous phase is different for all three nano-membrane thicknesses. This can be explained by the variation of material volume to which heat is transferred. From the results presented in Fig. 8 the values for the critical heat above which the material degrades (irreversibly) for such layered chalcogenides were determined as follows: ~ 17, ~ 23 and ~ 30 pJ for ~ 40, ~ 60 and ~ 90 nm thin $Ge_1Sb_2Te_4$ nano-membranes, respectively, and are marked with arrows in Fig. 8. After exceeding the critical heat values, irreversible structural changes in all three cases were observed. One possible effect, which certainly has a direct impact on the observed critical heat values, is the non-uniform distance between the nano-LEDs generating the optical pulses and the investigated nano-membrane materials. Fig. 1 presented a schematic of the ideal case i.e. if the nano-membrane is directly, mechanically in contact with the nano-LED testing platform. However, as it can be seen in Fig. 6(c), the phase changed areas are not all totally round but rather some are oval and, in addition, are not of the same size. This indicates, that the nano-membrane positioned above the nano-LED emitting area may be locally, mechanically deformed resulting in variations in the incident optical power and different optical power densities in the cases of individual nano-LED emitting units (conditioned and arranged in the arrays) and finally in the non-uniform distribution of the developed heat, which induced the phase change locally - not only its state, but also the total nano-membrane area. This is clearly demonstrated in Fig. 9 by representative micro-Raman mapping images. Indeed, the smallest area where we could observe a phase change in this study was in the range of ~ 300 nm in diameter (see Fig. 6(c)), which indicates that at least partially (in a few cases below 10 %) the mechanical contact between the emitting nano-LEDs and the nano-membrane was in the range below the emitting wavelength (near-field regime). In our previous work [37] we already introduced near-field nano-LED assisted lithography. The photo-chemical reactions were induced locally in a photosensitive film. After the subsequent developing process “hole” structures of about 75 nm were demonstrated.

Furthermore, as it can be seen from Fig. 9, several phase change modified nano-membrane regions monitored by the micro-Raman measurements are not located at exactly the same positions as their hexagonally arranged nano-LED emitting sources below them. This can be explained by an additional mechanical effect leading to a non-uniform contact to the underlying nano-LED emitting sources. Originally, i.e. before exposure to the nano-LEDs, the intrinsic nano-membrane defined and transferred from the native substrate to the host substrate is mechanically relaxed and the nano-membrane is in close contact with the nano-LEDs. The regions exposed to the nano-LEDs with a larger intensity gradually become amorphous indicated by a shift of the Raman mode from ~ 125 cm^{-1} to ~ 121 cm^{-1}. They locally expand their volume more than those subjected to a lower nano-LED intensity. This explains the observed displacement of the phase changed material position. This effect could be possibly used, in future, to induce locally non-uniformly distributed strain regions in PCM nano-membranes and in such a way to reach favorable “memory” effects in optical computing circuits or data storage architectures. Nevertheless, the presented data for the critical heat for all three investigated nano-membranes yielded important information. Especially as future optical computing architectures and very early stage single logic optical units (currently under development) based on such materials require clearly defined values for reliable long-term operation.

For the calculation of the minimal theoretical amount of heat necessary for a phase change state initialization from crystalline to amorphous we used the following equation: $Q_c = \rho \times V_N \times (c_P \times \Delta T + c_{Lat})$. Here, ρ is defined as the volumetric mass density of the individual phase change material, V_N is equal to the total nano-membrane volume.

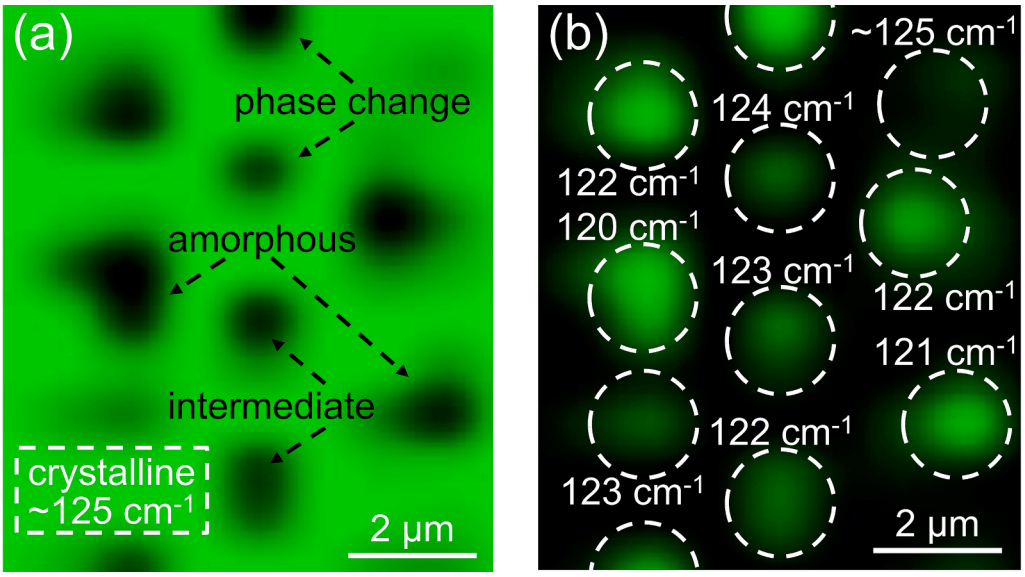

Fig. 9. Representative micro-Raman mapping images performed on the ~ 90 nm thin $Ge_1Sb_2Te_4$ nano-membrane at Raman modes: (a) 125 cm^{-1} and (b) in the range 120 ÷ 125 cm^{-1}. Micro-Raman mapping at 125 cm^{-1} (a) reveals that the crystalline state extends over a large area (green) in the $Ge_1Sb_2Te_4$ nano-membrane regions, which were not exposed to the nano-LEDs' optical pulses. High intensity relates to the color green, a change in phase to a low intensity (color black). Intermediate phase change states between the amorphous and crystalline are identified locally by micro-Raman mapping (b) in the range 120 ÷ 125 cm^{-1} (green marked regions). The phase change process was induced by optical pulses generated from the nano-LEDs integrated in the vertical device layout of which the final device testing platform is comprised of as presented in Fig. 3 (see 2. Experimental). (For interpretation of the references to colour in this figure legend, the reader is referred to the web version of this article.)

The mass $\rho \times V_N$ should remain constant during the phase change. c_P and c_{Lat} are the specific heat constant and the specific latent heat constant, respectively. The following parameters are inserted into the equation to calculate the heat necessary to induce the phase change. The density of the trigonal and of the amorphous $Ge_1Sb_2Te_4$ phase is 6.35 g cm^{-3} and 5.9 g cm^{-3}, respectively [77]. For simplification, the value for the specific heat was assumed to be constant and ~ 209 $Jkg^{-1}K^{-1}$ [78,79], in the temperature range under consideration i.e. $\Delta T \sim 150$ K [80]. Since the contribution of the latent heat to the phase change initialization heat is negligibly small [81], it is not included in the calculation. Taking into account the estimated average exposed area ~ 1 μm^2 (from Fig. 9) by a single nano-LED and for example a 100 nm thin $Ge_1Sb_2Te_4$ nano-membrane [20] the minimal theoretical heat level necessary for reaching the amorphous state (~120 cm^{-1}) should attain a heat level ~ 20 pJ. As it can be seen from Fig. 8, our measurements indicate rather higher heat levels (~ 10 pJ, ~ 18 pJ, and ~ 25 pJ for ~ 40, ~ 60 and ~ 90 nm thin nano-membranes) than the theoretically determined levels for our nano-membrane thicknesses. This result could be attributed to heat dissipation effects, since the island-like structures (defined locally in the nano-membrane after nano-LED exposure) are not spatially thermally isolated, but rather a part of a larger nano-membrane area (see Fig. 9).

In addition, the onset of phase change is dependent on the thickness of the membrane. First structural changes with Raman shifts around ~ 123 cm^{-1} evolve already at heat levels below 1 pJ for all three nano-membranes. A constant Raman shift for a specific phase i.e. the crystalline or the amorphous is observed independent of the nano-membrane thickness. The critical heat above which all three nano-membranes degrade was finally determined. The experimental results for the presented chalcogenide materials considered for future transmistor and/or all-optical switches devices indicate that the knowledge of minimal initialization heat as well as critical heat levels is crucial for long-term and reliable device operation.

Conclusions and outlook

We reported on the preparation of freestanding monocrystalline layered $Ge_1Sb_2Te_4$ nano-membranes with three different thicknesses (~40, ~ 60 and ~ 90 nm). They crystallize in the thermodynamically stable trigonal phase in the space group R $\bar{3}$m. Their properties with respect to phase change evolution were studied. To this end, nano-membranes were transferred to a device driving testing platform based on vertically integrated nano-LEDs, which were conditioned (locally annealed) to obtain different EL intensities. The platform allowed us to induce phase changes and to simultaneously observe their evolution by Raman spectroscopy. It was then employed as an effective tool for the determination of the critical heat in this optically active media. The results obtained can be summarized as follows:

(i) micro-Raman mapping at 125 cm^{-1} reveals that the crystalline state extends over a large area in the non-exposed $Ge_1Sb_2Te_4$ nano-membrane regions. Furthermore, nano-membrane regions exposed locally to the nano-LEDs' optical emission exhibit different phase change states from the crystalline, through intermediate states to the amorphous phase. A decrease of the Raman shift of the most intense Raman mode is observed from the crystalline phase (~ 125 cm^{-1}) to the amorphous phase (~ 120 cm^{-1}). This decrease was used to determine the minimal heat level at which the amorphous phase is reached for trigonal epitaxial $Ge_1Sb_2Te_4$ nano-membranes. The phase change process itself was induced by optical pulses both in the near- and far-field regime as demonstrated by the size of phase change modified lateral regions with a dimension from ~ 300 nm up to ~ 1.5 μm.

(ii) the starting point of phase change initialization i.e. the minimum heat was identified for all three layer thicknesses in the range below 1 pJ. Additionally, values of the critical heat for trigonal epitaxial $Ge_1Sb_2Te_4$ were determined as follows: ~ 17, ~ 23, ~ 30 pJ for ~ 40, ~ 60 and ~ 90 nm nano-membrane thicknesses, respectively.

The current achievements disclosed that optical pulses generated by nano-LED structures can induce substantial phase changes at the predefined $Ge_1Sb_2Te_4$ nano-membrane positions. Our results demonstrate the suitability and potential of the vertically integrated nano-LEDs as key components for an electro-optical testing platform to drive phase change processes in optically active media. This represents a significant step forward in the development of next generation transmistor based e.g. non-volatile data storage, optical and/or neuromorphic computing architectures.

Declaration of Competing Interest

The authors declare that they have no known competing financial interests or personal relationships that could have appeared to influence the work reported in this paper.

Data availability

Data will be made available on request.

Acknowledgments

The authors would like to acknowledge Prof. Z. Sofer (Institute of Chemical Technology, Prague, Czech Republic) for the technical support by epitaxial growth of the material and the use of laboratory facilities for fabrication of the presented testing platform / electro-optical convertors. MM and HHH are additionally grateful to A. Hardtdegen for his technical support and permission to use his homemade electrical pulse generator for the experiments presented in this study.

References

[1] G.W. Burr, M.J. Breitwisch, M. Franceschini, D. Garetto, K. Gopalakrishnan, B. Jackson, B. Kurdi, C. Lam, L.A. Lastras, A. Padilla, B. Rajendran, S. Raoux, R. S. Shenoy, Phase change memory technology, J. Vac. Sci. Technol. B Microelectron. Nanom. Struct. 28 (2010) 223, https://doi.org/10.1116/1.3301579.

[2] A.L. Lacaita, D.J. Wouters, Phase-change memories, Phys. Status Solidi. 205 (2008) 2281–2297, https://doi.org/10.1002/pssa.200723561.

[3] L. Polavarapu, S. Mourdikoudis, I. Pastoriza-Santos, J. Pérez-Juste, Nanocrystal engineering of noble metals and metal chalcogenides: controlling the morphology, composition and crystallinity, CrystEngComm. 17 (2015) 3727–3762, https://doi.org/10.1039/C5CE00112A.

[4] M. Wuttig, N. Yamada, Phase-change materials for rewriteable data storage, Nat. Mater. 6 (2007) 824–832, https://doi.org/10.1038/nmat2009.

[5] S. Mukhopadhyay, J. Sun, A. Subedi, T. Siegrist, D.J. Singh, Competing covalent and ionic bonding in Ge-Sb-Te phase change materials, Sci. Rep. 6 (2016) 25981, https://doi.org/10.1038/srep25981.

[6] C. Wu, H. Yu, H. Li, X. Zhang, I. Takeuchi, M. Li, Low-Loss Integrated Photonic Switch Using Subwavelength Patterned Phase Change Material, ACS Photonics. 6 (2019) 87–92, https://doi.org/10.1021/acsphotonics.8b01516.

[7] A. Lotnyk, M. Behrens, B. Rauschenbach, Phase change thin films for non-volatile memory applications, Nanoscale Adv. 1 (2019) 3836–3857, https://doi.org/10.1039/C9NA00366E.

[8] S. Moshfeghifar, K. Abbasian, M.M. Gilarlue, M.A.T.G. Jahani, Active tunable plasmonic switch designed by metal–insulator–metal waveguides connected to a nanodisk cavity enabled by a phase-change material ring, Opt. Eng. 60 (2021) 1–9, https://doi.org/10.1117/1.OE.60.4.045104.

[9] I. Vassalini, I. Alessandri, D. de Ceglia, Stimuli-Responsive Phase Change Materials: Optical and Optoelectronic Applications, Materials (Basel). 14 (2021) 3396, https://doi.org/10.3390/ma14123396.

[10] J. Zheng, S. Zhu, P. Xu, S. Dunham, A. Majumdar, Modeling Electrical Switching of Nonvolatile Phase-Change Integrated Nanophotonic Structures with Graphene Heaters, ACS Appl. Mater. Interfaces. 12 (2020) 21827–21836, https://doi.org/10.1021/acsami.0c02333.

[11] C. Rios, M. Stegmaier, Z. Cheng, N. Youngblood, C.D. Wright, W.H.P. Pernice, H. Bhaskaran, Controlled switching of phase-change materials by evanescent-field coupling in integrated photonics [Invited], Opt. Mater. Express. 8 (2018) 2455, https://doi.org/10.1364/OME.8.002455.

[12] S. Abdollahramezani, O. Hemmatyar, H. Taghinejad, A. Krasnok, Y. Kiarashinejad, M. Zandehshahvar, A. Alù, A. Adibi, Tunable nanophotonics enabled by chalcogenide phase-change materials, Nanophotonics. 9 (2020) 1189–1241, https://doi.org/10.1515/nanoph-2020-0039.

[13] Y. Zhang, J.B. Chou, J. Li, H. Li, Q. Du, A. Yadav, S. Zhou, M.Y. Shalaginov, Z. Fang, H. Zhong, C. Roberts, P. Robinson, B. Bohlin, C. Ríos, H. Lin, M. Kang, T. Gu, J. Warner, V. Liberman, K. Richardson, J. Hu, Broadband transparent optical phase change materials for high-performance nonvolatile photonics, Nat. Commun. 10 (2019) 4279, https://doi.org/10.1038/s41467-019-12196-4.

[14] L. Zhou, H. Zhang, L. Lu, J. Chen, Z. Zhou, B.M.A. Rahman, Ultra-Compact Multi-Level Optical Switching with Non-Volatile GST Phase Change, in: 2019 24th Optoelectron. Commun. Conf. 2019 Int. Conf. Photonics Switch. Comput., IEEE, 2019, pp. 1–3, https://doi.org/10.23919/PS.2019.8818027.

[15] M. Stegmaier, C. Ríos, H. Bhaskaran, C.D. Wright, W.H.P. Pernice, Nonvolatile All-Optical 1 × 2 Switch for Chipscale Photonic Networks, Adv. Opt. Mater. 5 (2017) 1600346, https://doi.org/10.1002/adom.201600346.

[16] M.N. Julian, C. Williams, S. Borg, S. Bartram, H.J. Kim, Reversible optical tuning of GeSbTe phase-change metasurface spectral filters for mid-wave infrared imaging, Optica. 7 (2020) 746, https://doi.org/10.1364/OPTICA.392878.

[17] W. Zhang, R. Mazzarello, M. Wuttig, E. Ma, Designing crystallization in phase-change materials for universal memory and neuro-inspired computing, Nat. Rev. Mater. 4 (2019) 150–168, https://doi.org/10.1038/s41578-018-0076-x.

[18] M. Suri, O. Bichler, D. Querlioz, O. Cueto, L. Perniola, V. Sousa, D. Vuillaume, C. Gamrat, B. DeSalvo, Phase change memory as synapse for ultra-dense neuromorphic systems: Application to complex visual pattern extraction, Tech. Dig. - Int. Electron Devices Meet. IEDM. (2011) 79–82, https://doi.org/10.1109/IEDM.2011.6131488.

[19] M. Mikulics, H. Hardtdegen, World Patent Application, Component having optically active materials, WO2020114532A1, 2019; Forschungszentrum Jülich GmbH.

[20] M. Mikulics, H.H. Hardtdegen, Fully photon operated transmistor / all-optical switch based on a layered $Ge_1Sb_2Te_4$ phase change medium, FlatChem. 23 (2020), 100186, https://doi.org/10.1016/j.flatc.2020.100186.

[21] M. Mikulics, J. Mayer, H.H. Hardtdegen, Cutting-edge nano-LED technology, J. Appl. Phys. 131 (2022), 110903, https://doi.org/10.1063/5.0087279.

[22] K.V. Mitrofanov, P. Fons, K. Makino, R. Terashima, T. Shimada, A.V. Kolobov, J. Tominaga, V. Bragaglia, A. Giussani, R. Calarco, H. Riechert, T. Sato, T. Katayama, K. Ogawa, T. Togashi, M. Yabashi, S. Wall, D. Brewe, M. Hase, Sub-nanometre resolution of atomic motion during electronic excitation in phase-change materials, Sci. Rep. 6 (2016) 20633, https://doi.org/10.1038/srep20633.

[23] S. Ovshinsky, Reversible electrical switching phenomena in disordered structures, Phys. Rev. Lett. 21 (1968), https://doi.org/10.1103/PhysRevLett.21.1450.

[24] A.V. Kolobov, P. Fons, A.I. Frenkel, A.L. Ankudinov, J. Tominaga, T. Uruga, Understanding the phase-change mechanism of rewritable optical media, Nat. Mater. 3 (2004) 703–708, https://doi.org/10.1038/nmat1215.

[25] T. Matsunaga, N. Yamada, Structural investigation of $GeSb_2Te_4$: A high-speed phase-change material, Phys. Rev. B. 69 (2004) 1–8, https://doi.org/10.1103/PhysRevB.69.104111.

[26] R. Gusmão, Z. Sofer, M. Pumera, Exfoliated Layered Manganese Trichalcogenide Phosphite ($MnPX_3$, X = S, Se) as Electrocatalytic van der Waals Materials for Hydrogen Evolution, Adv. Funct. Mater. 29 (2019) 1805975, https://doi.org/10.1002/adfm.201805975.

[27] J. Luxa, L. Spejchalová, I. Jakubec, Z. Sofer, MoS_2 stacking matters: 3R polytype significantly outperforms 2H MoS_2 for the hydrogen evolution reaction, Nanoscale. 13 (2021) 19391–19398, https://doi.org/10.1039/D1NR03284D.

[28] S. Supriya, N. Antonatos, J. Luxa, R. Gusmão, Z. Sofer, Comparison between layered Pt_3Te_4 and $PtTe_2$ for electrocatalytic reduction reactions, FlatChem. 29 (2021) 1–7, https://doi.org/10.1016/j.flatc.2021.100280.

[29] F.M. Oliveira, N. Antonatos, V. Mazánek, D. Sedmidubský, Z. Sofer, R. Gusmão, Exfoliated Fe_3GeTe_2 and Ni_3GeTe_2 materials as water splitting electrocatalysts, FlatChem. 32 (2022), https://doi.org/10.1016/j.flatc.2022.100334.

[30] K. Ishizaka, M.S. Bahramy, H. Murakawa, M. Sakano, T. Shimojima, T. Sonobe, K. Koizumi, S. Shin, H. Miyahara, A. Kimura, K. Miyamoto, T. Okuda, H. Namatame, M. Taniguchi, R. Arita, N. Nagaosa, K. Kobayashi, Y. Murakami, R. Kumai, Y. Kaneko, Y. Onose, Y. Tokura, Giant Rashba-type spin splitting in bulk BiTeI, Nat. Mater. 10 (2011) 521–526, https://doi.org/10.1038/nmat3051.

[31] R. Li, Y. Cheng, W. Huang, Recent Progress of Janus 2D Transition Metal Chalcogenides: From Theory to Experiments, Small. 14 (2018) 1802091, https://doi.org/10.1002/smll.201802091.

[32] M. Schuck, S. Rieß, M. Schreiber, G. Mussler, D. Grützmacher, H. Hardtdegen, Metal organic vapor phase epitaxy of hexagonal Ge–Sb–Te (GST), J. Cryst. Growth. 420 (2015) 37–41, https://doi.org/10.1016/j.jcrysgro.2015.03.034.

[33] H. Hardtdegen, S. Rieß, M. Schuck, K. Keller, P. Jost, H. Du, M. Bornhöfft, A. Schwedt, G. Mussler, M.v.d. Ahe, J. Mayer, G. Roth, D. Grützmacher, M. Mikulics, A model structure for interfacial phase change memories: Epitaxial trigonal $Ge_1Sb_2Te_4$, J. Alloys Compd. 679 (2016) 285–292, https://doi.org/10.1016/j.jallcom.2016.04.013.

[34] M. Mikulics, M. Marso, R. Adam, M. Schuck, A. Fox, R. Sobolewski, P. Kordos, H. Luth, D. Grutzmacher, H. Hardtdegen, Electrical and optical characterization of freestanding $Ge_1Sb_2Te_4$ nano-membranes integrated in coplanar strip lines, in: 2016 11th Int. Conf. Adv. Semicond. Devices Microsystems, IEEE, 2016, pp. 73–76.

[35] J. Wang, F. Sciarrino, A. Laing, M.G. Thompson, Integrated photonic quantum technologies, Nat. Photonics. 14 (2020) 273–284, https://doi.org/10.1038/s41566-019-0532-1.

[36] K. Kluczyk-Korch, D. Palazzo, A. Waag, A. Diéguez, J.D. Prades, A. Di Carlo, M. A. der Maur, Optical design of InGaN/GaN nanoLED arrays on a chip: toward: highly resolved illumination, Nanotechnology. 32 (2021), 105203, https://doi.org/10.1088/1361-6528/abcd60.

[37] M. Mikulics, Z. Sofer, A. Winden, S. Trellenkamp, B. Förster, J. Mayer, H. H. Hardtdegen, Nano-LED induced chemical reactions for structuring processes, Nanoscale Adv. 2 (2020) 5421–5427, https://doi.org/10.1039/D0NA00851F.

[38] M. Mikulics, Y.C. Arango, A. Winden, R. Adam, A. Hardtdegen, D. Grützmacher, E. Plinski, D. Gregušová, J. Novák, P. Kordoš, A. Moonshiram, M. Marso, Z. Sofer, H. Lüth, H. Hardtdegen, Direct electro-optical pumping for hybrid CdSe nanocrystal/III-nitride based nano-light-emitting diodes, Appl. Phys. Lett. 108 (2016), 061107, https://doi.org/10.1063/1.4941923.

[39] M. Mikulics, A. Winden, M. Marso, A. Moonshiram, H. Lüth, D. Grützmacher, H. Hardtdegen, Nano-light-emitting-diodes based on InGaN mesoscopic structures for energy saving optoelectronics, Appl. Phys. Lett. 109 (2016), 041103, https://doi.org/10.1063/1.4960007.

[40] A. Winden, M. Mikulics, A. Haab, D. Grützmacher, H. Hardtdegen, Spectral sensitivity tuning of vertical InN nanopyramid-based photodetectors, Jpn. J. Appl. Phys. 52 (2013) 08JF05, https://doi.org/10.7567/JJAP.52.08JF05.

[41] Z.J. Liu, T. Huang, J. Ma, C. Liu, K.M. Lau, Monolithic Integration of AlGaN/GaN HEMT on LED by MOCVD, IEEE Electron Device Lett. 35 (2014) 330–332, https://doi.org/10.1109/LED.2014.2300897.

[42] Y. Cai, X. Zou, C. Liu, K.M. Lau, Voltage-Controlled GaN HEMT-LED Devices as Fast-Switching and Dimmable Light Emitters, IEEE Electron Device Lett. 39 (2018) 224–227, https://doi.org/10.1109/LED.2017.2781247.

[43] Y. Wang, X. Wang, B. Zhu, Z. Shi, J. Yuan, X. Gao, Y. Liu, X. Sun, D. Li, H. Amano, Full-duplex light communication with a monolithic multicomponent system, Light Sci. Appl. 7 (2018) 83, https://doi.org/10.1038/s41377-018-0083-0.

[44] M. Mahdizadeh Rokhi, A. Asgari, Power improvement in ridge bent waveguide superluminescent light-emitting diodes based on GaN quantum dots, Phys. Scr. 96 (2021), 125520, https://doi.org/10.1088/1402-4896/ac33fc.

[45] A. Macková, P. Malinský, A. Jagerová, Z. Sofer, K. Klímová, D. Sedmidubský, M. Pristovsek, M. Mikulics, J. Lorinčík, R. Böttger, S. Akhmadaliev, Structural and optical properties of Gd implanted GaN with various crystallographic orientations, Thin Solid Films. 638 (2017) 63–72, https://doi.org/10.1016/j.tsf.2017.07.036.

[46] Y. Jiang, P. Liu, Y. Wang, Experimental Demonstration and Theoretical Analysis of Simultaneous Emission-Detection Phenomenon, ACS Omega. 7 (2022) 14017–14021, https://doi.org/10.1021/acsomega.2c00562.

[47] M.S. Khan, M. Ikram, L.-J. Shi, B. Zou, H. Ullah, M.Y. Khan, Computational insights into optoelectronic and magnetic properties of V(III)-doped GaN, J. Solid State Chem. 304 (2021), 122606, https://doi.org/10.1016/j.jssc.2021.122606.

[48] T. Hu, X. Li, C. Liu, S. Lin, K. Wang, J. Liu, L. Zhao, High performance conical nanostructured GaN-based photodetectors, J. Phys. D. Appl. Phys. 55 (2022), 035102, https://doi.org/10.1088/1361-6463/ac2cad.

[49] D. Priante, R.T. Elafandy, A. Prabaswara, B. Janjua, C. Zhao, M.S. Alias, M. Tangi, Y. Alaskar, A.M. Albadri, A.Y. Alyamani, T.K. Ng, B.S. Ooi, Diode junction temperature in ultraviolet AlGaN quantum-disks-in-nanowires, J. Appl. Phys. 124 (2018), 015702, https://doi.org/10.1063/1.5026650.

[50] D. Priante, in: Study of ultraviolet AlGaN nanowires light-emitting diodes, King Abdullah University of Science and Technology, 2019, https://doi.org/10.25781/KAUST-94563.

[51] Y. Liu, Q. Lu, G. Lin, J. Liu, S. Lu, Z. Tang, H. He, Y. Fu, X. Shen, Effect of thermal annealing on properties of amorphous GaN/p-Si heterojunctions, Mater. Res. Express. 6 (2019), 085904, https://doi.org/10.1088/2053-1591/ab1d0c.

[52] K. Kluczyk-Korch, S. Moreno, J. Canals, A. Diéguez, J. Gülink, J. Hartmann, A. Waag, A. Di Carlo, M. Auf der Maur, Individually Switchable InGaN/GaN Nano-LED Arrays as Highly Resolved Illumination Engines, Electronics. 10 (2021) 1829, https://doi.org/10.3390/electronics10151829.

[53] Y. Zhao, H. Wang, W. Zhang, J. Li, Y. Shen, Z. Huang, J. Zhang, A. Dingsun, Controllable process of nanostructured GaN by maskless inductively coupled plasma (ICP) etching, J. Micromech. Microeng. 27 (2017), 115004, https://doi.org/10.1088/1361-6439/aa8c4f.

[54] H.-Y. Lee, Y.-H. Ju, J.-I. Chyi, C.-T. Lee, Performance Comparison of Lattice-Matched AlInN/GaN/AlGaN/GaN Double-Channel Metal–Oxide–Semiconductor High-Electron Mobility Transistors with Planar Channel and Multiple-Mesa-Fin-Channel Array, Materials (Basel). 15 (2021) 42, https://doi.org/10.3390/ma15010042.

[55] L. Wang, X. Li, X. Gao, B. Jia, Q. Guan, Z. Ye, K. Fu, R. Jin, Y. Wang, Asymmetric optical links using monolithic III-nitride diodes, Opt. Lett. 46 (2021) 376, https://doi.org/10.1364/OL.415007.

[56] H.-Y. Lee, C.-H. Lin, C.-T. Lee, Fabrication and Characterization of AlGaN/GaN Enhancement-Mode MOSHEMTs With Fin-Channel Array and Hybrid Gate-Recessed Structure and $LiNbO_3$ Ferroelectric Charge Trap Gate-Stack Structure, IEEE Trans. Electron Devices. 69 (2022) 500–506, https://doi.org/10.1109/TED.2021.3133385.

[57] H.-Y. Lee, T.-W. Chang, E.Y. Chang, N. Rorsman, C.-T. Lee, Fabrication and Characterization of GaN-Based Fin-Channel Array Metal-Oxide-Semiconductor High-Electron Mobility Transistors With Recessed-Gate and Ga_2O_3 Gate Insulator Layer, IEEE J. Electron Devices Soc. 9 (2021) 393–399, https://doi.org/10.1109/JEDS.2021.3069973.

[58] M. Madhulika, A. Malik, P. Kamboj, S. Awasthi, P. Thakur, N. Jain, M. Mishra, S. Kumar, D.S. Rawal, A.K. Singh, Nanoscale material parameters based modeling of thermal noise in GaN HEMTs, Semicond. Sci. Technol. 36 (2020), https://doi.org/10.1088/1361-6641/abd265.

[59] M.Y. Chernykh, A.A. Andreev, I.S. Ezubchenko, I.A. Chernykh, I.O. Mayboroda, E. M. Kolobkova, Y.V. Khrapovitskaya, J.V. Grishchenko, P.A. Perminov, V.S. Sedov, A.K. Martyanov, A.S. Altakhov, M.S. Komlenok, V.P. Pashinin, A.G. Sinogeykin, V. I. Konov, M.L. Zanaveskin, GaN-based heterostructures with CVD diamond heat sinks: A new fabrication approach towards efficient electronic devices, Appl. Mater. Today. 26 (2022), 101338, https://doi.org/10.1016/j.apmt.2021.101338.

[60] Y. Liu, S. Chen, Z. Cheng, T. Wang, C. Huang, G. Jiang, H. Zhang, Y. Cai, Temperature dependence of the strain of the AlGaN barrier layer under the gate in AlGaN/AlN/GaN HFETs, Micro Nanostruct. 164 (2022), 107160, https://doi.org/10.1016/j.spmi.2022.107160.

[61] N. Bhardwaj, B.B. Upadhyay, Y.K. Yadav, S. Surapaneni, S. Ganguly, D. Saha, Thermally grown Nb-oxide for GaN-based MOS-diodes, Appl. Surf. Sci. 572 (2022), 151332, https://doi.org/10.1016/j.apsusc.2021.151332.

[62] M. Xie, F. Hu, C. Ma, Y. Jiang, Z. Shi, X. Gao, B. Jia, J. Yuan, H. Zhu, N. Chi, Y. Wang, 580-nm-thick vertical-structure light-emitting diode for visible light communication, Appl. Phys. Lett. 120 (2022), 181109, https://doi.org/10.1063/5.0088846.

[63] M. Mikulics, P. Kordoš, D. Gregušová, Z. Sofer, A. Winden, S. Trellenkamp, J. Moers, J. Mayer, H. Hardtdegen, Conditioning nano-LEDs in arrays by laser-micro-annealing: The key to their performance improvement, Appl. Phys. Lett. 118 (2021), 043101, https://doi.org/10.1063/5.0038070.

[64] M. Mikulics, J.G. Lu, L. Huang, P.L. Tse, J.Z. Zhang, J. Mayer, H. Hardtdegen, Laser micro annealing conditioning for the suppression of statistical scatter in freestanding Sb_2Te_3 nanowire resistance, FlatChem. 21 (2020), 100164, https://doi.org/10.1016/j.flatc.2020.100164.

[65] A. Dutta, K. Sathiyan, D. Sharon, A. Borenstein, Laser induced incorporation of CNTs in graphene electrodes improves flexibility and conductivity, FlatChem. 33 (2022), 100378, https://doi.org/10.1016/j.flatc.2022.100378.

[66] M. Mikulics, J. Zhang, J. Serafini, R. Adam, D. Grützmacher, R. Sobolewski, Subpicosecond electron-hole recombination time and terahertz-bandwidth photoresponse in freestanding GaAs epitaxial mesoscopic structures, Appl. Phys. Lett. 101 (2012), 031111, https://doi.org/10.1063/1.4737442.

[67] M. Mikulics, H. Hardtdegen, R. Adam, D. Grützmacher, D. Gregušová, J. Novák, P. Kordoš, Z. Sofer, J. Serafini, J. Zhang, R. Sobolewski, M. Marso, Impact of thermal annealing on nonequilibrium carrier dynamics in single-crystal, freestanding GaAs mesostructures, Semicond. Sci. Technol. 29 (2014), https://doi.org/10.1088/0268-1242/29/4/045022.

[68] R. Adam, M. Mikulics, A. Förster, J. Schelten, M. Siegel, P. Kordoš, X. Zheng, S. Wu, R. Sobolewski, Fabrication and subpicosecond optical response of low-temperature-grown GaAs freestanding photoconductive devices, Appl. Phys. Lett. 81 (2002) 3485–3487, https://doi.org/10.1063/1.1518159.

[69] M. Mikulics, X. Zheng, R. Adam, R. Sobolewski, P. Kordoš, High-speed photoconductive switch based on low-temperature GaAs transferred on SiO_2-Si substrate, IEEE Photonics Technol. Lett. 15 (2003) 528–530, https://doi.org/10.1109/LPT.2003.809264.

[70] M. Mikulics, R. Adam, M. Marso, A. Forster, P. Kordos, H. Luth, S. Wu, X. Zheng, R. Sobolewski, Ultrafast low-temperature-grown epitaxial GaAs photodetectors transferred on flexible plastic substrates, IEEE Photonics Technol. Lett. 17 (2005) 1725–1727, https://doi.org/10.1109/LPT.2005.851025.

[71] M. Marso, M. Mikulics, R. Adam, S. Wu, X. Zheng, I. Camara, F. Siebe, A. Förster, R. Güsten, P. Kordoš, R. Sobolewski, Ultrafast Phenomena in Freestanding LT-GaAs Devices, Acta Phys. Pol. A. 107 (2005) 109–117, https://doi.org/10.12693/APhysPolA.107.109.

[72] M. Mikulics, P. Kordoš, D. Gregušová, Š. Gaži, J. Novák, Z. Sofer, J. Mayer, H. Hardtdegen, Local increase in compressive strain (GaN) in gate recessed AlGaN/GaN MISHFET structures induced by an amorphous AlN dielectric layer, Semicond. Sci. Technol. 36 (2021), 095040, https://doi.org/10.1088/1361-6641/ac1a28.

[73] C. Ríos, M. Stegmaier, P. Hosseini, D. Wang, T. Scherer, C.D. Wright, H. Bhaskaran, W.H.P. Pernice, Integrated all-photonic non-volatile multi-level memory, Nat. Photonics. 9 (2015) 725–732, https://doi.org/10.1038/nphoton.2015.182.

[74] P. Němec, V. Nazabal, A. Moreac, J. Gutwirth, L. Beneš, M. Frumar, Amorphous and crystallized Ge–Sb–Te thin films deposited by pulsed laser: Local structure using Raman scattering spectroscopy, Mater. Chem. Phys. 136 (2012) 935–941, https://doi.org/10.1016/j.matchemphys.2012.08.024.

[75] A.V. Kolobov, M. Krbal, P. Fons, J. Tominaga, T. Uruga, Distortion-triggered loss of long-range order in solids with bonding energy hierarchy, Nat. Chem. 3 (2011) 311–316, https://doi.org/10.1038/nchem.1007.

[76] B. Kalkan, S. Sen, S.M. Clark, Nature of phase transitions in crystalline and amorphous GeTe-Sb_2Te_3 phase change materials, J. Chem. Phys. Appl. Phys. Lett. Phys. Lett. J. Appl. Phys. Appl. Phys. Lett. J. Appl. Phys. J. Chem. Phys. 135 (2011) 124510–232101, https://doi.org/10.1063/1.2956409.

[77] T. Blachowicz, M.G. Beghi, G. Güntherodt, B. Beschoten, H. Dieker, M. Wuttig, Crystalline phases in the $GeSb_2Te_4$ alloy system: Phase transitions and elastic properties, J. Appl. Phys. 102 (2007), 093519, https://doi.org/10.1063/1.2809355.

[78] B. Hyot, V. Gehanno, B. Rolland, A. Fargeix, C. Vannufel, F. Charlet, B. Béchevet, J. M. Bruneau, P.J. Desre, Amorphization and Crystallization mechanisms in GeSbTe-based Phase Change Optical Disks, J. Magn. Soc. Japan. 25 (2001) 414–419, https://doi.org/10.3379/jmsjmag.25.414.

[79] P.K. Khulbe, X. Xun, M. Mansuripur, Crystallization and amorphization studies of a $Ge_2Sb_{2.3}Te_5$ thin-film sample under pulsed laser irradiation, Appl. Opt. 39 (2000) 2359, https://doi.org/10.1364/AO.39.002359.

[80] L. Xu, L. Tong, L. Geng, F. Yang, J. Xu, W. Su, D. Liu, Z. Ma, K. Chen, A comparative study on electrical transport properties of thin films of $Ge_1Sb_2Te_4$ and $Ge_2Sb_2Te_5$ phase-change materials, J. Appl. Phys. 110 (2011), 013703, https://doi.org/10.1063/1.3603016.

[81] J. Scoggin, R.S. Khan, H. Silva, A. Gokirmak, Modeling and impacts of the latent heat of phase change and specific heat for phase change materials, Appl. Phys. Lett. 112 (2018), 193502, https://doi.org/10.1063/1.5025331.